Journal of Zhejiang University-SCIENCE A (Applied Physics & Engineering)
ISSN 1673-565X (Print); ISSN 1862-1775 (Online)
www.jzus.zju.edu.cn; www.springerlink.com
E-mail: jzus@zju.edu.cn

A reduced and optimized kinetic mechanism for coke oven gas as a clean alternative vehicle fuel*

Hai-bin HE, Dong-wei YAO†‡, Feng WU

(*Institute of Power Machinery and Vehicular Engineering, Zhejiang University, Hangzhou 310027, China*)

†E-mail: dwyao@zju.edu.cn

Received Sept. 21, 2016; Revision accepted Jan. 19, 2017; Crosschecked June 12, 2017

Abstract: A reduced and optimized kinetic mechanism was built for coke oven gas (COG) as a clean alternative vehicle fuel. This mechanism was constructed by combining a reduced methane mechanism, an optimized H_2/CO mechanism, and a reduced NO_x formation mechanism based on the mechanism structure for simple hydrocarbon fuels. The key reactions for combustion were investigated by a sensitivity analysis model, and the kinetic parameters of these reactions were optimized within the uncertainty range by an optimization model based on particle swarm optimization (PSO). The ignition delay time and laminar flame speed were simulated using the optimized mechanism with the software of CHEMKIN, and the results agreed well with the relevant experimental data. A computational fluid dynamics (CFD) model coupled with the optimized mechanism was established using KIVA-CHEMKIN software, and the in-cylinder combustion process was simulated. The simulation results (in-cylinder pressure and NO_x emission) showed good agreement with the engine bench test results.

Key words: Coke oven gas (COG); Kinetic mechanism; Sensitivity analysis; Particle swarm optimization (PSO); Spark-ignition (SI) engine; Computational fluid dynamics (CFD) simulation

http://dx.doi.org/10.1631/jzus.A1600636 **CLC number:** TK432

1 Introduction

The kinetic mechanism plays a very important role in the simulation of combustion for the internal combustion (IC) engine, such as flame propagation, heat release and emissions (Turns, 1996; Ra and Reitz, 2008). Nowadays, with the decrease of conventional fossil sources and the increase of environmental pollutions, clean alternative vehicle fuels have attracted more and more attention. Coke oven gas (COG) is one of the main by-products in the process of coking, and mainly contains hydrogen (55% to 60%), methane (23% to 27%), and carbon monoxide (5% to 8%). Given its high content of hydrogen and methane, it becomes one of the most realistic options as a clean alternative vehicle fuel (He *et al*., 2013). However, if the spark-ignition (SI) engine is fueled with COG directly, some problems such as higher NO_x emission, lower engine power, and higher probability of knock will occur (Shioji *et al*., 2004). Computational fluid dynamics (CFD) simulation is an appropriate way to investigate the engine performance, especially coupled with kinetic mechanisms (Qin *et al*., 2014). Therefore, it is an urgent matter to investigate the application of COG in IC engines.

Since the 1980s, several methodologies for mechanism reduction and optimization were proposed in the literature. Sensitivity analysis proposed by Rabitz *et al*. (1983) is one of the earliest reduction methods, and it is simple to understand and apply, but fails to directly simplify a mechanism with high accuracy. Hence, it is always used as a supplementary

‡ Corresponding author

* Project supported by the Major Project of Guizhou Province (No. 2012(6001)), China

ORCID: Hai-bin HE, http://orcid.org/0000-0002-1225-0272; Dong-wei YAO, http://orcid.org/0000-0001-7698-514X

means in other optimization methods. The reaction elimination method (Bhattacharjee *et al*., 2003) can reduce the mechanism by identifying the optimal reactions, but the identification speed is much slower than that in sensitivity analysis. Detailed reduction (Wang and Frenklach, 1991) is used to identify the unimportant reactions based on the direct comparisons of reaction rates, and the optimization process is accelerated by the preselected critical values. However, the reduced size is highly dependent on the computational capability. Chemical lumping (Ahmed *et al*., 2007) simplifies mechanisms by replacing the isomeric species with lumped pseudo species. Based on the pre-calculated reactor experimental data, the simplification process can be performed strictly mathematically. However, when the number of isomeric species is large, the analysis will be complicated or even fail. The direct relation graph method (DRGM) (Lu and Law, 2006) can identify the unimportant species with high efficiency based on the internal relationships, but it is not easy to acquire, and extra algorithms need to be applied to reduce the calculation time when the number of species is large. Particle swarm optimization (PSO) is a relatively new kind of evolutionary algorithm (EA) introduced by Kennedy and Eberhart (1995). It can find the optimal solution by random searching and iterative calculation, and the global optimal solution will be found through the current optimal solution without crossover and mutation, while the quality of solution is evaluated by the fitness. Therefore, PSO is an excellent algorithm because of its advantages such as easy implementation, high accuracy, and fast convergence. Combined with sensitivity analysis, PSO becomes a kind of computer aided reduction method (CARM) (Montgomery *et al*., 2002), which can reduce and optimize mechanisms automatically with a high accuracy.

Based on these methods, many mechanisms have been constructed and optimized. Boni and Penner (1977), Sher and Refael (1988), Bilger *et al*. (1990), Smooke (1991), and Jazbec *et al*. (2000) proposed different reduced mechanisms for methane combustion, and they all led to similar good agreement with experimental flame speed data. Davis *et al*. (2005), Saxena and Williams (2006), Frassoldati *et al*. (2007), Li *et al*. (2007), and Sun *et al*. (2007) proposed several updated H_2/CO mechanisms, and they all predicted reaction time scales similarly over comparable pressure and temperature ranges (Kalitan *et al*., 2007; Petersen *et al*., 2007). However, until now, no kinetic mechanism for COG has been put forward, and the detailed methane combustion model was always used in the COG simulations. Consequently, in the process of CFD simulation, a lot of computational resources were occupied, while results with low accuracy were simulated. Therefore, it is necessary to propose a reduced and optimized kinetic mechanism for COG to reduce the computational cost and improve the simulation accuracy.

In this study, a reduced and optimized mechanism for COG was developed. As a multi-component mechanism, it was constructed by combining reduced methane, optimized H_2/CO and reduced NO_x formation mechanisms. In this mechanism, the key reactions for combustion were studied by a sensitivity analysis model, and their kinetic parameters were optimized by the mechanism optimization model based on PSO. Subsequently, several experimental data were used to validate the optimized mechanism: the ignition delay time was validated by shock-tube experimental data, while the laminar flame speed was validated by the premixed flame data. In addition, the applicability of the mechanism under engine-relevant conditions was investigated by a CFD in-cylinder model coupled with the optimized mechanism. This model was established by the KIVA-CHEMKIN software, and the simulation results were validated by the experimental data from the engine test bench.

2 Construction and optimization of COG mechanism

2.1 Methodology for mechanism construction

In this study, we regarded the gas mixture of hydrogen, methane, and carbon monoxide as COG. The construction process is shown in Fig. 1, and the detailed procedure is summarized in steps 1–4.

Step 1 Constructing the reduced methane mechanism

Methane is the simplest and most widely used hydrocarbon fuel, and a lot of detailed mechanisms have been proposed, for instance, GRI-Mech 3.0 (Smith *et al*., 1999), Konnov mechanism (Konnov, 2000), Leads mechanism (Hughes *et al*., 2001), Williams mechanism (Li and Williams, 2002), and Warnatz mechanism (Warnatz, 2000). In this study, GRI-Mech 3.0 was chosen as the detailed methane

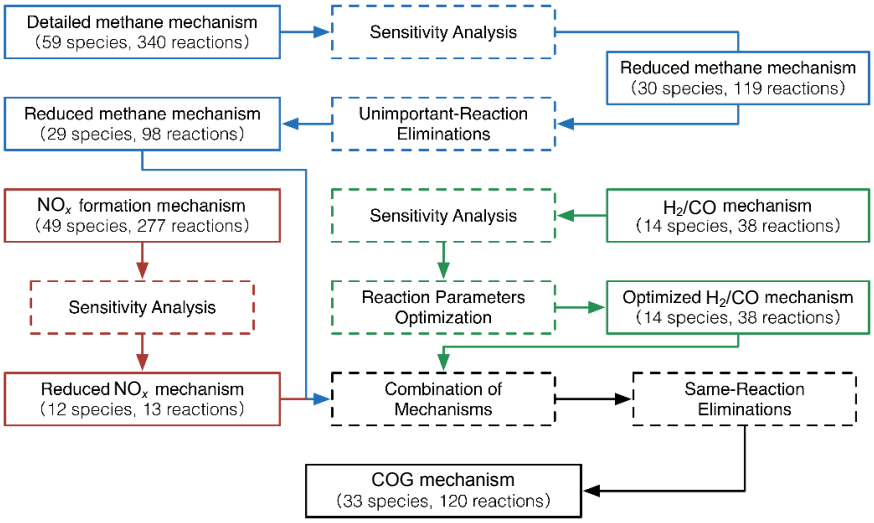

Fig. 1 Construction process of COG mechanism

mechanism. It is the most recognized mechanism for methane all over the world. However, only conditions under high-temperature and low-pressure were validated for GRI-Mech 3.0, and it becomes inaccurate under engine-relevant conditions. In order to solve this problem, 6 species and 15 reactions were incorporated into GRI-Mech 3.0 (Huang *et al*., 2004; Petersen *et al*., 1999), shown in Appendix A, and the final detailed methane mechanism contained 59 species and 340 reactions. Based on sensitivity analysis and unimportant-reaction eliminations, a reduced methane kinetic mechanism was proposed, which contained 29 species and 98 reactions.

Step 2 Choosing an optimized H_2/CO mechanism

Based on careful comparison of kinetic parameters and a lot of experimental data, a H_2/CO combustion model was proposed by Mueller *et al*. (1999). It used to be the most successful H_2/CO combustion model, but failed to predict the combustion characteristics accurately with the developments of rate parameters, third-body efficiencies, and enthalpies of different species (Ruscic *et al*., 2001; Michael *et al*., 2002). In recent times, several new H_2/CO combustion mechanisms were published, and the agreement between measurements and simulations were investigated by Olm *et al*. (2015). In this study, after careful comparison, the optimized model proposed by Davis *et al*. (2005) was chosen as one part of the COG mechanism, which was developed on the basis of revised thermodynamic data under high temperature, and validated over a wide range of conditions.

Step 3 Choosing a reduced NO_x formation mechanism

Because of the high hydrogen content, a higher in-cylinder temperature will be observed, which is advantageous to the formation of NO_x. Therefore, the NO_x formation is very important in COG mechanism. Bowman (1992) classified NO_x formation into three categories: the extended Zeldovich (or thermal) mechanism in which O, OH, and N_2 species are at their equilibrium values and N atoms are in steady state; mechanisms whereby NO is formed more rapidly than predicated by the thermal mechanism; a fuel nitrogen mechanism in which fuel-bound nitrogen is converted to NO. In this study, the reduced NO_x formation mechanism proposed by Golovitchev (2002) was chosen, and tested to be accurate in the SI engine simulation.

Step 4 Combining mechanisms

Based on the mechanism structure for simple hydrocarbon fuels (Kuo, 1986), the reduced methane, optimized H_2/CO, and reduced NO_x formation mechanisms were integrated into the COG mechanism. During the process of combination, 29 reactions with the same reaction equation but different kinetic parameters were observed from the reduced methane mechanism and optimized H_2/CO mechanism. In order to ensure the accuracy of mechanism, the duplicate reactions from the reduced methane mechanism were deleted.

In summary, the COG mechanism constructed above consists of three parts: a reduced methane

kinetic mechanism (containing 29 species and 98 reactions), an optimized H_2/CO mechanism (containing 14 species and 38 reactions) and a reduced NO_x formation mechanism (containing 12 species and 13 reactions). It contains 33 species and 120 reactions after combination. Details can be found in Appendix B.

2.2 Sensitivity analysis

Using sensitivity analysis (Rabitz *et al*., 1983), the sensitivity of components, basic reactions, and reaction conditions to the changes of reaction parameters can be deeply and directly analyzed. Therefore, it is often used for the reduction and optimization of kinetic mechanisms.

In this study, sensitivity analysis was used to discover the most sensitive reactions for ignition delay time and laminar flame speed.

The ignition delay time sensitivity was defined as

$$S_{ij}=\frac{\tau_{2k_j}-\tau_{k_j}}{\tau_{k_j}}, \tag{1}$$

where S_{ij} is the ignition delay time sensitivity of reaction j; τ is the ignition delay time; k_j is the reaction rate constant of reaction j.

The laminar flame speed sensitivity was defined as

$$S_{fj}=\frac{\mathrm{Su}_{2k_j}-\mathrm{Su}_{k_j}}{\mathrm{Su}_{k_j}}, \tag{2}$$

where S_{fj} is the laminar flame speed sensitivity of reaction j, and Su is the laminar flame speed.

Based on CHEMKIN (Kee *et al*., 1996) code and their definitions, the ignition delay time sensitivity analysis was conducted using the constant volume (CONV) model, which was employed with the constant volume and energy assumption, and the laminar flame speed sensitivity was calculated using the PREMIX (Kee *et al*., 1985) model.

By running the ignition delay time sensitivity model, the ignition delay time sensitivities of hydrogen, methane, carbon monoxide (CO/H_2=0.99/0.01 in volume), and COG ($H_2/CH_4/CO$=0.6/0.3/0.1) at different initial temperatures T of 950, 1000, and 1050 K are shown in Fig. 2, and the temperatures are chosen on the basis of Mittal *et al*. (2006). The initial pressure P is 20 bar (1 bar=100 kPa) and the initial equivalence ratio Φ is 1. R1: $H+O_2=O+OH$ and R22: $H_2O_2+H=HO_2+H_2$ play important roles in the ignition delay time of hydrogen and COG. R82: $CH_3+H_2O_2=$

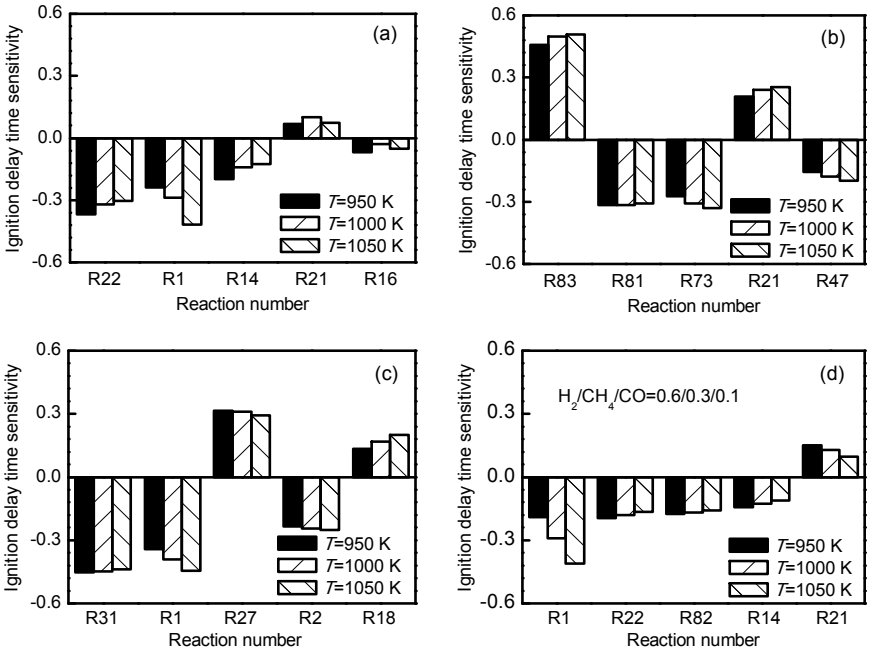

Fig. 2 Ignition delay time sensitivity of COG mechanism with different temperatures of T=950 K, 1000 K, and 1050 K (other initial conditions of the calculation were P=20 bar and Φ=1): (a) H_2; (b) CH_4; (c) CO; (d) $H_2/CH_4/CO$

HO_2+CH_4 has a significant effect on the ignition delay time of COG. In addition, R83: $2CH_3(+M)=C_2H_6(+M)$ is the key reaction for the ignition delay time of methane, and R31: $CO+HO_2=CO_2+OH$ is the key reaction for the ignition delay time of carbon monoxide.

By running the laminar flame speed sensitivity model, the laminar flame speed sensitivities of hydrogen, methane, carbon monoxide (CO/H_2= 0.99/0.01), and COG ($H_2/CH_4/CO$=0.6/0.3/0.1) with different equivalence ratios of 0.8, 1.0, and 1.2 are calculated and shown in Fig. 3. The initial pressure is 1 bar and the initial temperature is 298 K. R3: $OH+H_2=H+H_2O$ is the key reaction for the laminar flame speed of hydrogen, and R1: $H+O_2=O+OH$ is the key reaction for the laminar flame speed of methane and COG. R28 and R29 are two reactions with the same chemical reaction equation but different kinetic parameters ($CO+OH=CO_2+H$), and they are both the key reactions for the laminar flame speed of carbon monoxide.

2.3 Particle swarm optimization (PSO)

PSO is an optimized evolutionary algorithm developed by Kennedy and Eberhart (1995) on the basis of swarm intelligence. It has been widely used in the fields of calculation and control. In order to get better accuracy for the simulation of combustion characteristics, some kinetic parameters can be optimized by PSO based on the sensitivity analysis and experimental data. In this study, an algorithm called RPSO (Liu *et al*., 2007) was applied to avoid the optimization falling into a local optimal solution, and to improve the running efficiency and precision of overall optimization searching during evolution calculation. The process of RPSO is shown in Fig. 4.

In this algorithm, a swarm consists of m particles placed in the target searching space with a dimension of d. Then the position of each particle is evaluated using a specific indicator, and the best position of the current swarm as well as the best position of all swarms are identified. Based on these two positions, the movement velocity can be calculated with some random perturbations, and the position of particles in the next swarm can be determined. The movement velocity and the next position of the particle can be described as:

$$v_{id}(t+1)=c_1r_1[p_{\text{best}id}(t)-p_{id}(t)]+c_2r_2[g_{\text{best}id}(t)-p_{id}(t)]+wv_{id}(t), \tag{3}$$

$$p_{id}(t+1)=p_{id}(t)+v_{id}(t+1), \tag{4}$$

where v is the movement velocity and p is the particle position; i is the number of particles in the swarm and d is the dimensionality of the searching space; c_1 and

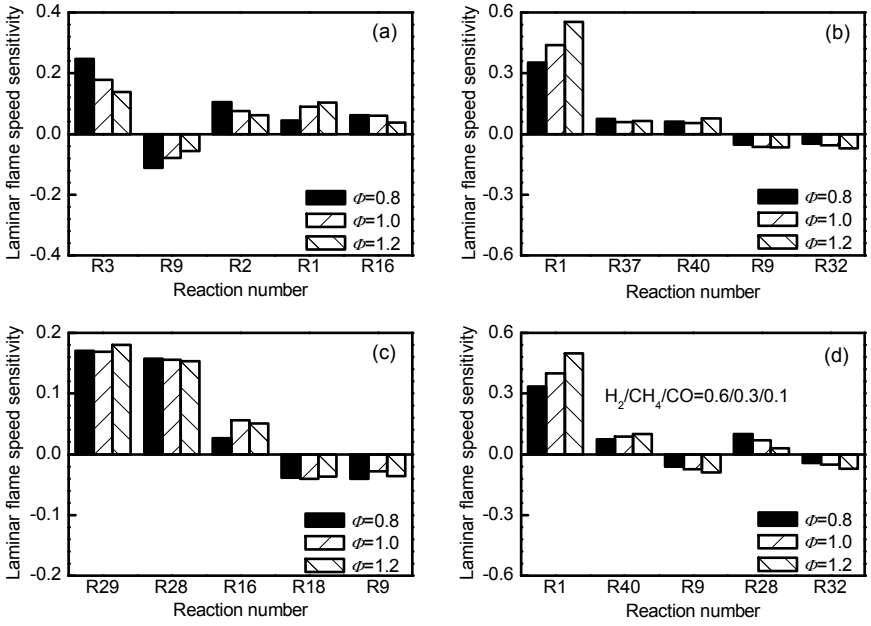

Fig. 3 Laminar flame speed sensitivity of COG mechanism with different equivalence ratios of Φ=0.8, 1.0, and 1.2 (other initial conditions of the calculation were P=1 bar and T=298 K): (a) H_2; (b) CH_4; (c) CO; (d) $H_2/CH_4/CO$

c_2 are study parameters ($c_1 \geq 0$, $c_2 \geq 0$); r_1 and r_2 are random perturbations, and $r_1, r_2 \in [0, 1]$; w is an inertia factor, and $w \in [0.3, 0.9]$; p_{best} is the best function result in the swarm and g_{best} is the best function result for all swarms that have been calculated.

The convergence degree of the particle swarm is described as the standard deviation of the swarm:

$$\alpha = \sqrt{\frac{1}{m}\sum_{i=1}^{m}(f_i - f_{\text{average}})^2}, \tag{5}$$

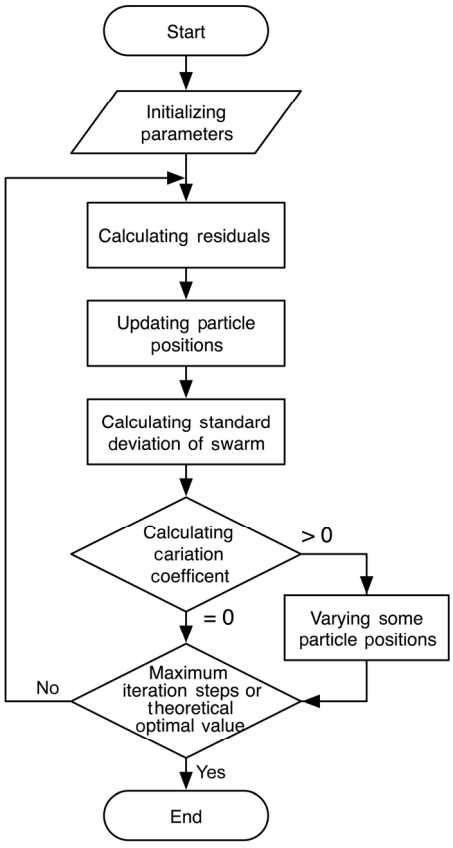

Fig. 4 Flow chart of RPSO

where f_i is the residual of particle i, and f_{average} is the average residual of the current swarm. If the convergence degree is small, then the optimization is going to converge. Otherwise, the particle swarm optimization is in a state of random search.

In order to judge if the optimization has fallen into a local optimal solution or not, the mutation parameter q is introduced:

$$q = \begin{cases} k, & (\alpha < \alpha_{\text{v}}) \cap (f_{\text{gbest}} > f_{\text{best}}), \\ 0, & (\alpha \geq \alpha_{\text{v}}) \cup (f_{\text{gbest}} \leq f_{\text{best}}), \end{cases} \tag{6}$$

where k is the mutation probability, and $k \in (0, 1)$; α is the convergence degree; α_{v} is the threshold of convergence degree; f_{gbest} is the residual of the particle with global optimal value; f_{best} is the residual of the particle with a theoretically optimal value.

When the optimization falls into a local optimal solution, then the following mutation algorithm will be used to help it to jump out:

$$p_{id} = p_{id}(0.62\mu + 1), \tag{7}$$

where μ is a random number, $\mu \in (-1, 1)$.

At the same time, in order not to destroy any good characteristics that the swarm has achieved, only Int(m/2) particles will be mutated.

In order to guarantee the accuracy of the mechanism, the kinetic parameters have to be optimized within the uncertainty range. In this study, the uncertainties for the key reactions were calculated by the method described by Varga *et al*. (2011) and Turányi *et al*. (2012), and all the direct measurements were collected from the NIST Chemical Kinetics Database and the literature (Baulch *et al*., 1994). The uncertainties of reactions are shown in Fig. 5, where the

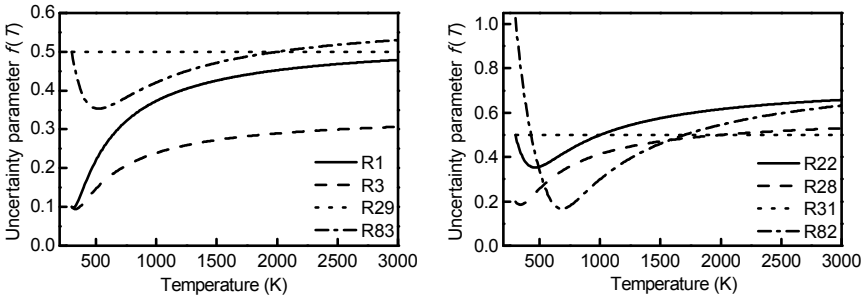

Fig. 5 Uncertainties for the reactions considered in the optimization

uncertainties of R29 and R31 were estimated to be 0.5, because little information for them can be found in the literature.

The kinetic parameters of R1, R3, R22, R28, R29, R31, R82, and R83 were optimized by RPSO, and all the experimental data used in the optimization are shown in Table 1. The revised reaction parameters can be found in Appendix C. The final optimized COG mechanism is named COG-Mech.

3 Validation

The ignition delay time and laminar flame speed are two important characteristics in the combustion process, and they are important indicators for validating the accuracy of the kinetic mechanism. In this study, the ignition delay time and laminar flame speed were simulated with the mechanisms of GRI-Mech 3.0 and COG-Mech, and the simulation results were analyzed and compared with the experimental data in the literature.

3.1 Validation of ignition delay time

Shock tube (Gaydon and Hurle, 1963) is a method commonly used to measure ignition delay times, with a lot of research and experimental data published. In this study, a 0D model of ignition delay time was built using the CONV model from CHEMKIN code, and the ignition delay time was defined as the time between ignition and maximal temperature rise rate. Subsequently, the ignition delay times of hydrogen, methane, carbon monoxide, and their mixtures were calculated, and the comparisons between simulation results and experimental data obtained from the literature are shown in Figs. 6–9.

An indicator named average error was defined to evaluate the accuracy of the mechanism:

$$\mathrm{Err}=\frac{1}{N}\sum_{i=1}^{N}\mathrm{abs}(\lg\tau_{\mathrm{e},i}-\lg\tau_{\mathrm{c},i}), \tag{8}$$

where Err is the average error, N is the number of experimental data points, τ_{e} is the measured ignition delay time (ms), and τ_{c} is the simulated ignition delay time (ms).

Comparisons for the ignition delay time of methane at the pressures of 16–40 bar and temperature of 298 K between simulation and experimental results are presented in Fig. 6. The results simulated by COG-Mech show a good agreement with the experimental data from the study of Huang *et al*. (2004). The reversed-'S'-shape characteristic and the negative temperature coefficient (NTC) region, which have been shown in the results of Huang *et al*. (2004) and Petersen *et al*. (1999), can be correctly simulated: when the temperature decreased, the activation energy reduced at the same time, but re-increased when the temperature decreased below 1100 K. However, GRI-Mech 3.0 appears to over-predict ignition delay times in all conditions, and fails to predict the change of activation energy.

Fig. 7 presents the simulated and measured ignition delay times for hydrogen at the pressures of 15–50 bar and temperature of 298 K. The trend of ignition delay time with temperature observed from the experiments can be simulated by these two mechanisms (Mittal *et al*., 2006). However, GRI-Mech 3.0 appears to over-predict the ignition delays at high temperatures, but under-predict the ignition delays at low temperatures. COG-Mech shows better agreement with the present experimental data.

Table 1 Experimental data used in the optimization

Item	Fuel	Diluent	Φ	P (bar)	T (K)
Ignition delay time	H_2	N_2/Ar	1	30	950/1000/1050
	CH_4	N_2	1	30	1035/1184/1296
	CO/H_2=0.2/0.8	N_2/Ar	1	30	1010.5
	CO/H_2=0.6/0.4	N_2/Ar	1	30	1010.5
Laminar flame speed	H_2	N_2	0.9/1.8/3	1	298
	CH_4	N_2	0.9/1.1/1.2	1	300
	H_2/CO/NG=3/1/1	N_2	0.8/1/1.2	1	298

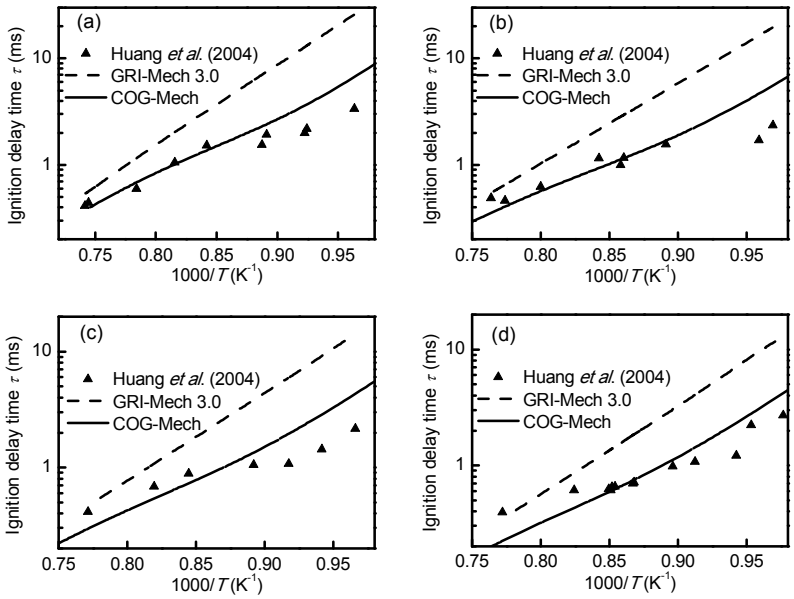

Fig. 6 Comparison of ignition delay times for methane between simulation and experimental data under different pressures of *P*≈16 bar (a), *P*≈23 bar (b), *P*≈30 bar (c), and *P*≈40 bar (d)

Molar composition: $CH_4/O_2/N_2$=9.5/19/71.5; symbols were the experimental data from Huang *et al*. (2004)

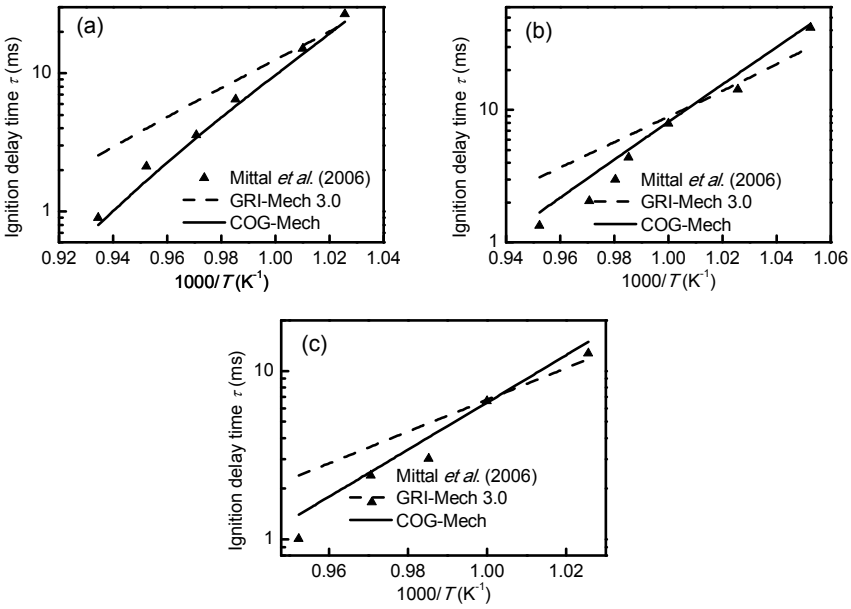

Fig. 7 Comparison of ignition delay times for hydrogen between simulation and experimental data under different pressures of *P*≈15 bar (a), *P*≈30 bar (b), and *P*≈50 bar (c)

Molar composition: $H_2/O_2/N_2/Ar$=12.5/6.25/18.125/63.125; symbols were the experimental data from Mittal *et al*. (2006)

Fig. 8 presents the experimental data of ignition delay times for H_2/CO mixtures as a function of R_{CO}, which is defined as the volume fraction of CO in the mixtures (Mittal *et al*., 2006), as well as the simulated results calculated with two different mechanisms. The function of CO for the auto-ignition of H_2/CO mixtures is also investigated. Clearly an inhibition function of CO addition is observed, and a longer ignition delay time is measured with the increase of R_{CO}. However, GRI-Mech 3.0 fails to simulate the

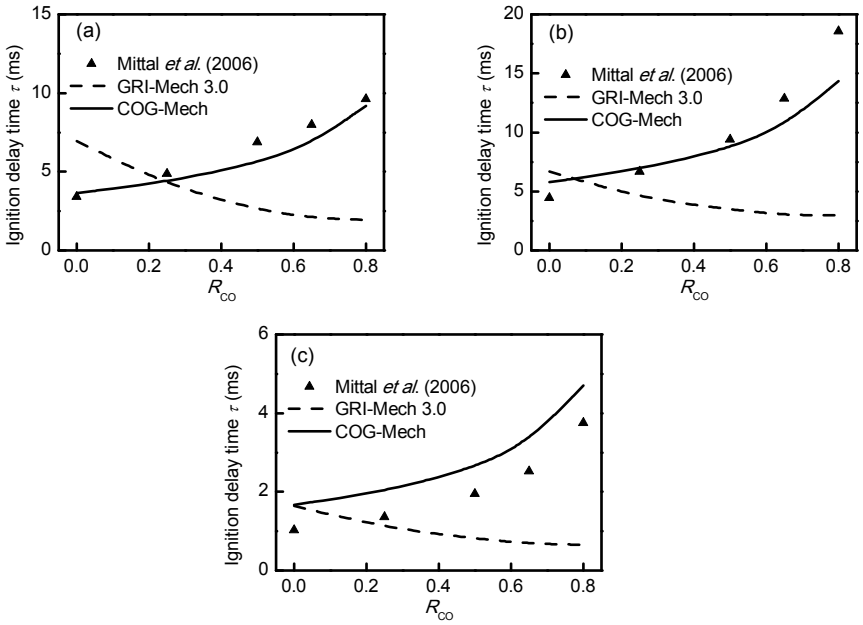

Fig. 8 Comparison of ignition delay times for H_2/CO between simulation and experimental data (Mittal *et al*., 2006) under different conditions: (a) *P*=15 bar, *T*=1028.5 K; (b) *P*=30 bar, *T*=1010.5 K; (c) *P*=50 bar, *T*=1044 K

Molar composition: $(H_2+CO)/O_2/N_2/Ar=12.5/6.25/18.125/63.125$; R_{CO}: volume fraction of CO

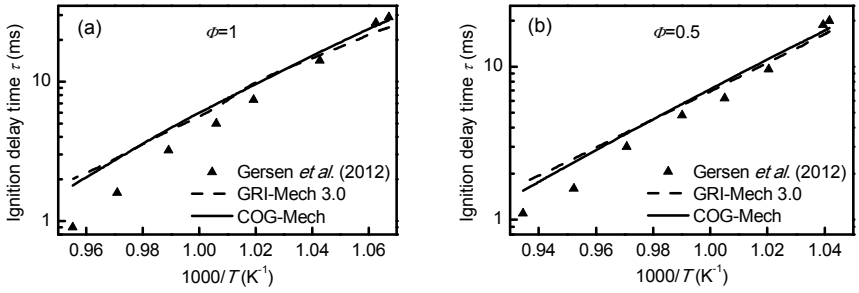

Fig. 9 Comparison of ignition delay times for H_2/CH_4/CO between simulation and experimental data (Gersen *et al*., 2012) under different conditions of *P*≈40 bar (a) and *P*≈50 bar (b)

Molar composition: (a) $H_2/CH_4/CO/O_2/N_2/Ar=4.1/6.9/2.8/17.2/30/39$; (b) $H_2/CH_4/CO/O_2/N_2/Ar=2.2/3.7/1.5/1$

inhibition effect of CO addition, and an opposite trend is observed. COG-Mech has good agreement with the experimental data, and it can accurately predict the inhibition effect of CO.

Fig. 9 presents the measured and calculated auto-ignition delay times of $CH_4/H_2/CO$ mixtures as a function of temperature at the pressures of 40 and 50 bar. Under these two conditions, shown in the study of Gersen *et al*. (2012), both mechanisms can accurately simulate the trend of ignition delay time with temperature, and their simulation results are quite close to each other, a little over-predicting at high temperatures and slightly under-predicting at low temperatures. The Err of COG-Mech is 0.117, a little better than GRI-Mech 3.0, whose Err is 0.128.

All the comparisons above indicate that COG-Mech, as constructed and optimized in this study, can predict the ignition delay time of different fuels more accurately over a wide range of conditions than the GRI-Mech 3.0, the most commonly used mechanism, especially for predicting the NTC of methane and the inhibition effect of CO addition. However, in some cases, some significant differences still exist between the simulated and experimental results. This may because in the process of reduction only the important reaction pathways were retained, and the main

oxidation process was affected. Therefore, some further kinetic studies should be carried out, and the kinetic parameters can be further optimized.

3.2 Validation of laminar flame speed

Laminar flame speed, a fundamental combustion characteristic of fuels, can significantly affect the burning rate in IC engines, and consequently affect engine performance and emissions (Metghalchi and Keck, 1980; Dong *et al*., 2009). Many methods have been devised to measure the laminar flame speed of fuels, such as the Mach Hebra nozzle burner, the Bunsen burner, spherically expanding flame, flat flame, and counter flow flame (Huang *et al*., 2006). In this study, a 1D model of laminar flame speed was developed using the PREMIX model in CHEMKIN code, and the simulation results of various fuels, calculated with different mechanisms, were compared with the experimental data from the literature. However, because of the technical limits and characteristics of fuels, it is difficult to acquire reliable experimental data for laminar flame speed under high pressure and temperature, especially for the hydrogen blended fuels, where the highly explosive nature of hydrogen makes the measurements of laminar flame speed very difficult.

The measured and simulated laminar flame speed as a function of fuel equivalence ratio for hydrogen, methane, and carbon monoxide are presented and compared in Fig. 10. As commonly used fuels, a lot of research has been done to measure their laminar flame speed (Scholte and Vaags, 1959; Dowdy *et al*., 1991; Davis and Law, 1998; Gu *et al*., 2000; Kwon and Faeth, 2001; Krejci *et al*., 2013; Dong *et al*., 2014). Under atmospheric pressure, hydrogen has the maximum laminar flame speed of 286 cm/s at the equivalence ratio of 1.8, while methane has the maximum laminar flame of 38.8 cm/s at the equivalence ratio of 1.05, and carbon monoxide has the maximum laminar flame speed of 28 cm/s at the equivalence ratio of 2.85. With increasing pressure, flame speeds decrease markedly. For example, the maximum laminar flame speed of methane decreases from 38.8 cm/s to 15 cm/s when the pressure is increased to 5 bar. The calculated flame speeds using GRI-Mech 3.0 and COG-Mech show reasonable

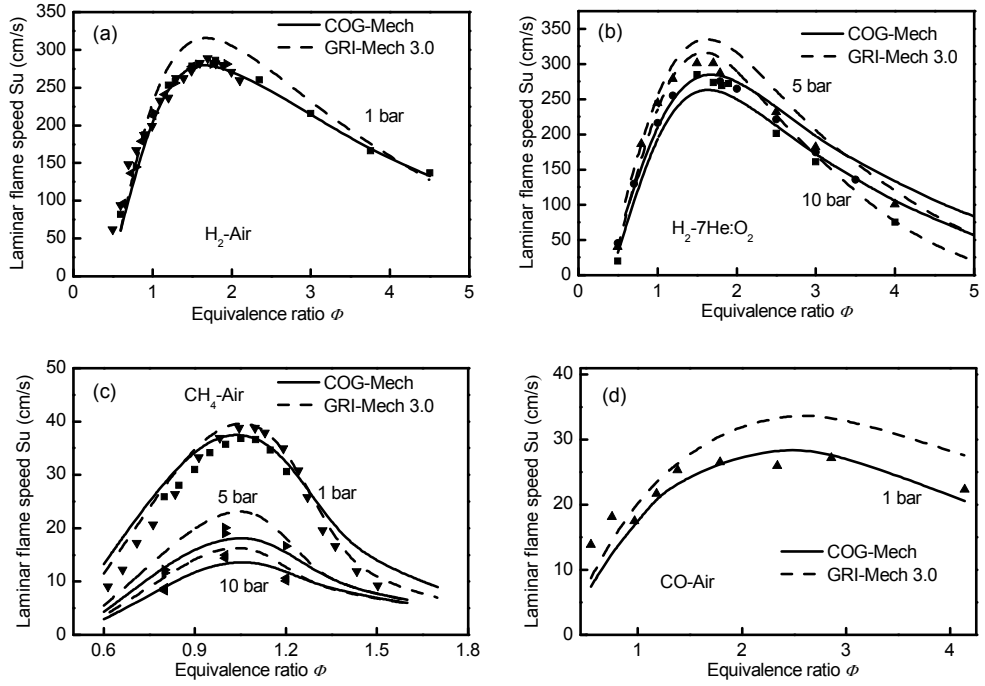

Fig. 10 Comparison of laminar flame speed for: (a) H_2 (P=1 bar, T=298 K); (b) H_2 (P=5, 10 bar, T=298 K); (c) CH_4 (P=1, 5, 10 bar, T≈298 K); (d) CO (P=1 bar, T=298 K)

Molar composition of CO: $CO/N_2/O_2/CH_4/H_2$=98.53/0.6/0.3/0.02/0.55; Symbols were the experimental data (Scholte and Vaags, 1959; Dowdy *et al*., 1991; Davis and Law, 1998; Gu *et al*., 2000; Kwon and Faeth, 2001; Krejci *et al*., 2013; Dong *et al*., 2014)

agreement with the experimental data, while GRI-Mech 3.0 appears to slightly over-predict the flame speeds in all conditions.

In Fig. 11, the comparisons of calculated and measured laminar flame speeds (Sun *et al*. 2007) for H_2/CO/Air and H_2/CO/O_2/He mixtures as a function of equivalence ratio at pressures of 1–10 bar are shown. With the increase of hydrogen blend ratio, the laminar flame speed increases simultaneously, while the equivalence ratio for the maximal laminar flame speed decreases. For example, under atmospheric pressure, when the hydrogen blend ratio is 1%, the maximal laminar flame speed of 36 cm/s appears at the equivalence ratio of 2.85, and the maximal laminar flame speed increases to 186 cm/s at the equivalence ratio of 1.8 when the hydrogen ratio increases to 50%. Both mechanisms can indicate the rules of laminar flame speed for H_2/CO mixtures, but the calculated results by GRI-Meh 3.0 are much larger than the experimental data, and the error becomes even larger with the increase of hydrogen blend ratio. This is mainly because of the over-prediction of GRI-Mech 3.0 in the simulation of laminar flame speed for hydrogen. Therefore, COG-Mech has better agreement with experimental results in the simulation of laminar flame speed for H_2/CO mixtures.

In Fig. 12, the laminar flame speeds measured (Halter *et al*., 2005) and calculated for CH_4/H_2/Air mixtures at the pressures of 1–5 bar and temperature of 298 K are plotted. For both mixtures, the same pressure dependence is observed, and adequately described by the mechanisms. Furthermore, the results calculated by COG-Mech have better agreement with the measurements, while GRI-Mech 3.0 appears to over-predict the flame speeds in all conditions.

In Fig. 13, numerical results for the flame speed of H_2/CH_4/CO mixtures are compared with the experimental results at the pressure of 1 bar, where little experimental data under high pressures can be found in the literature because of the difficulty in measurement. Dong *et al*. (2014) measured the laminar flame speed of seven H_2/CH_4/CO mixtures with a Bunsen burner in both lean and rich conditions. Both mechanisms can accurately reflect the trend of flame speed: increase with the volumetric fraction of hydrogen or carbon monoxide, and decrease with the volumetric fraction of methane. However, the simulation results using GRI-Mech 3.0 are slightly bigger than the experimental data in all conditions, while the simulation results using COG-Mech have good agreement with the experimental data around the stoichiometric equivalence ratio (Φ=0.6–1.2), but

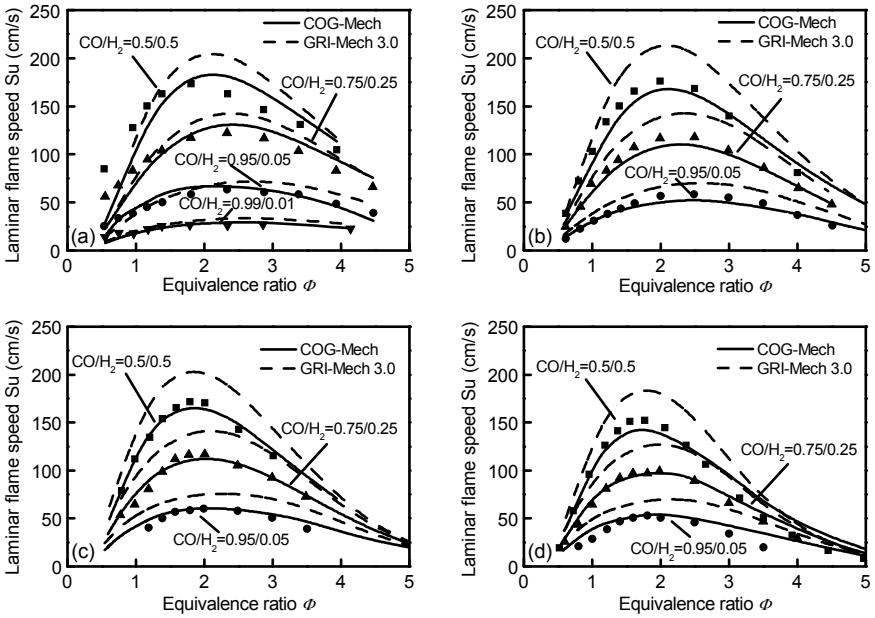

Fig. 11 Comparison of laminar flame speed for CO/H_2 mixtures under the pressures of P=1 bar (a), P=2 bar (b), P=5 bar (c), and P=10 bar (d), and temperature of 298 K

Symbols were the experimental data from Sun *et al*. (2007)

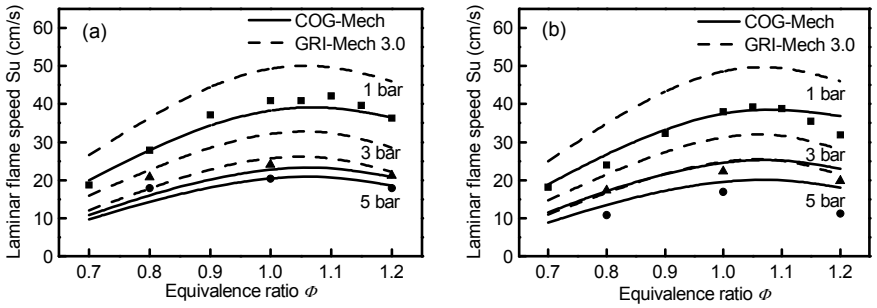

Fig. 12 Comparison of laminar flame speed for CH_4/H_2 mixtures under the pressures of 1, 3, 5 bar and initial temperature of 298 K: (a) $CH_4/H_2/O_2/N_2$=0.9/0.1/1.85/6.96; (b) $CH_4/H_2/O_2/N_2$=0.8/0.2/1.7/6.40
Symbols were the experimental data from Halter *et al*. (2005)

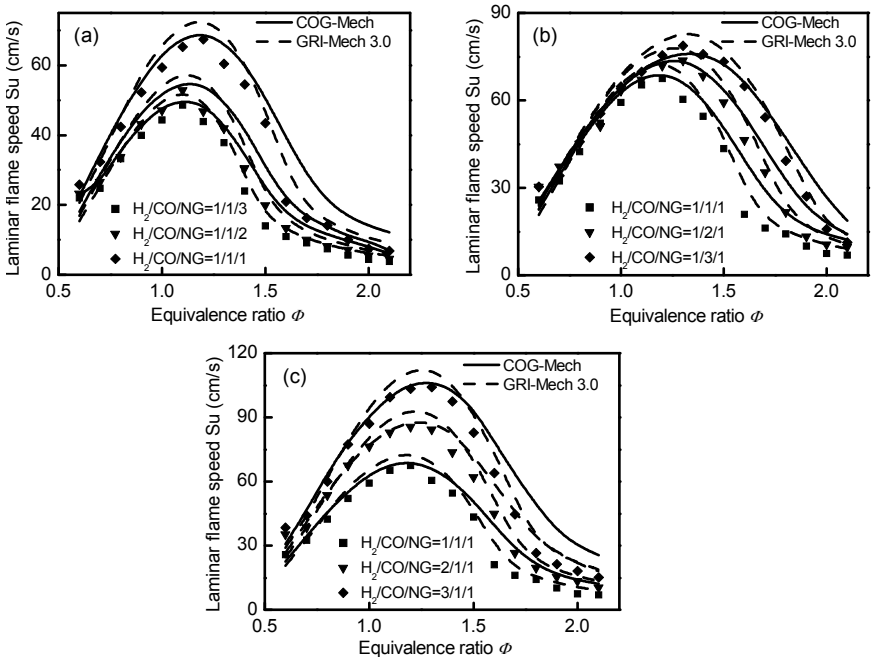

Fig. 13 Comparison of laminar flame speed for H_2/CO/NG under the pressure of 1 bar and initial temperature of 298 K
NG: natural gas; Symbols were the experimental data from Dong *et al*. (2014)

become a little bigger than the experimental data when the equivalence ratio is bigger than 1.2. The reason can be found by analyzing the laminar flame speed sensitivity, which is shown in Fig. 3. For the flame speed of H_2/CH_4/CO mixtures, the dominant reaction is R1: $H+O_2=O+OH$, the most important chain reaction, and it becomes even more important when the equivalence ratio increases. Therefore, when the equivalence ratio increases to 1.2, COG-Mech becomes a little over-predicting, and the kinetic parameters can be further optimized.

Although some discrepancies exist between simulated and experimental results in cases of different gas mixtures, the trends can be accurately simulated. In order to guarantee the high efficiency of three way catalytic (TWC) converters, the engines with port fuel injection (PFI) always work under stoichiometric conditions. Therefore, the laminar flame speed around the stoichiometric equivalence ratio is very important, and COG-Mech is accurate enough for the simulation of SI engines.

In all cases, the laminar flame speed increases with the increase of temperature or the decrease of pressure. Based on this, the variation of laminar flame speed with temperature and pressure can be expressed through the empirical expression (Metghalchi and

Keck, 1980):

$$\mathrm{Su}=\mathrm{Su}_0\left(\frac{T_u}{T_0}\right)^{\alpha_T}\left(\frac{P_u}{P_0}\right)^{\beta_P}, \tag{9}$$

where Su_0 is the laminar flame speed at a datum temperature and pressure of T_0 and P_0. In most studies, 298 K and 1 bar are chosen for T_0 and P_0. T_u and P_u are the temperature and pressure of unburned gas, respectively. α_T and β_P are two parameters dependent upon the equivalence ratio, and a lot of work has been done to define their values for different fuels (Gu *et al*., 2000; Halter *et al*., 2005; Bougrine *et al*., 2011). Therefore, the laminar flame speed under datum temperature and pressure is very important in the validation of laminar flame speed.

3.3 Validation with engine experiments

In order to evaluate the applicability of COG-Mech in engine simulations, a 3D CFD model was established with KIVA-CHEMKIN, and the in-cylinder combustion process was simulated. The engine grids include the combustion chamber and intake/exhaust ports were meshed on the basis of an SI engine, and the detailed structure parameters are shown in Table 2, while the visual meshes are shown in Fig. 14. Moreover, in order to improve the simulation accuracy of the spark ignition process in SI engines, a developed discrete particle ignition kernel (DPIK) model was applied (Tan and Reitz, 2006).

An engine test bench was established on the basis of a COG engine, which was developed from a gasoline SI engine named MR479q. The layout of the engine testing system is shown in Fig. 15. The engine fuel of COG was obtained by mixing hydrogen, methane, and carbon monoxide in specific volume proportions. In this study, the volume fraction of hydrogen in COG is 0.575, while the methane is 0.25, and the carbon monoxide is 0.175. During the measurements, a combustion analyzer produced by DEWETRON was used to record the in-cylinder pressure and heat release. In order to capture the details of pressure fluctuations, the sampling period was set to 0.1 °CA, and more than 200 cycles were

Table 2 Engine parameters for simulation

Parameter	Value
Bore (mm)	78.7
Stroke (mm)	69
Connecting rod length (mm)	122
Compression ratio	9.3

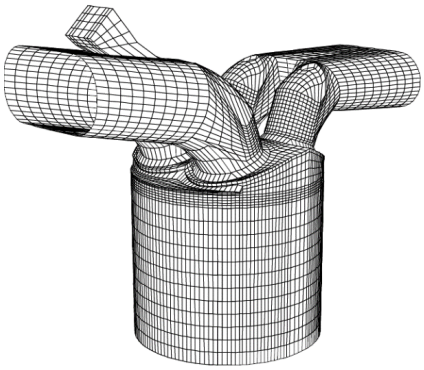

Fig. 14 Computational mesh used in engine simulations

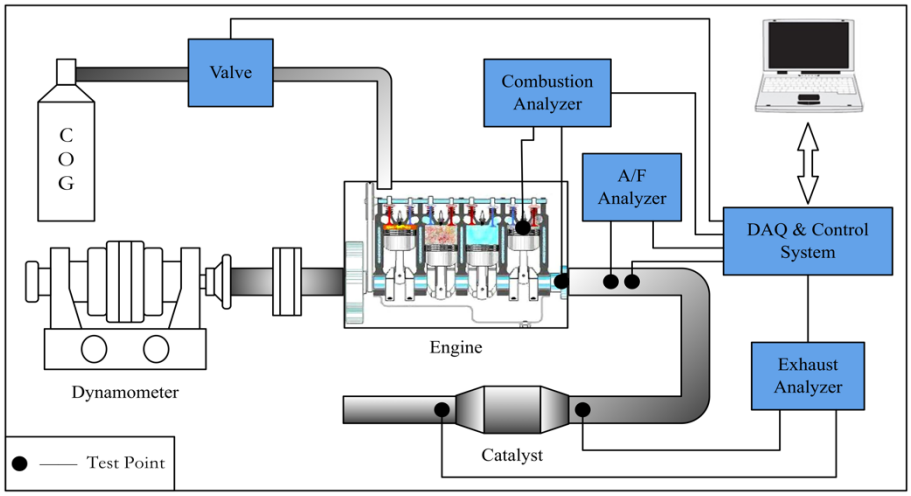

Fig. 15 Layout of engine testing system (A/F: air-fuel ratio; DAQ: data acquisition)

recorded for every condition. A Fourier transform infrared (FTIR) spectrometer produced by AVL, Austria was used to measure the engine emissions, and the sampling frequency is 2 Hz and sampling precision is one part per million of volume fraction. Therefore, after calibration, the deviation of NO measured in the test can be controlled within 3%.

Fig. 16 shows the comparisons of in-cylinder pressure between experimental data and simulation results at two different engine conditions. The experimental in-cylinder pressure was based on the average values of at least 200 engine cycles. As shown in Fig. 16, the two curves are almost coincident, while the start of combustion is a little delayed and the top pressure of the simulation is a little larger than the experimental data. In general, the comparison indicates that COG-Mech can accurately describe the combustion process of a COG engine.

Fig. 17 shows the emission characteristics of NO_x under different conditions. The main composition of NO_x is NO under engine conditions, and the mole fraction of NO is chosen as the index of NO_x emission in this study. In Fig. 17, the mean mole fraction of NO inside the cylinder was carefully described, and the process can be summarized into 3 stages: a rapidly increasing stage, when the temperature is high enough and the concentration of oxygen is rich at the start of combustion; a gradually reducing stage, when the free radicals for chemical reactions are consumed fast; a stabilization stage after the free radicals are used up, and the concentration of NO becomes stable. The NO emissions obtained from the simulation results are a little lower than the experimental data measured at the exhaust pipe, but the error is smaller than 10%. The NO emission increases with the advance of ignition timing mainly because of the increase of temperature. Therefore, coupling with COG-Mech, the emission of NO_x can be accurately predicted.

Above all, with COG-Mech, the 3D CFD model can successfully simulate the process of in-cylinder combustion and NO_x formation.

4 Conclusions

In this study, a reduced kinetic mechanism for COG as a clean alternative vehicle fuel was developed

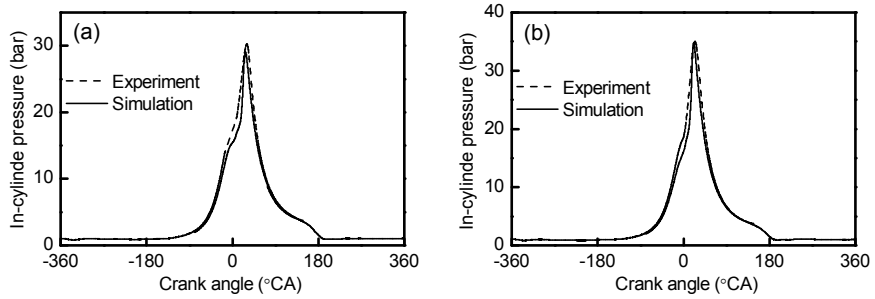

Fig. 16 Comparison of in-cylinder pressure between the simulation and experimental results: (a) 1600 r/min; 4 °CA BTDC; (b) 1600 r/min, 8 °CA BTDC (BTDC means before top dead center)

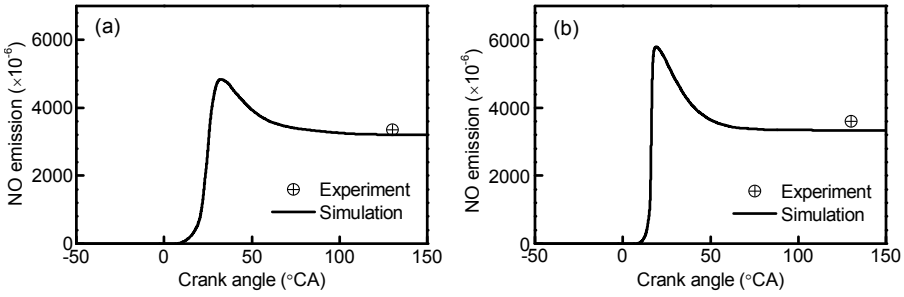

Fig. 17 Comparison of NO_x emission between the simulation and experimental results: (a) 1600 r/min, 4 °CA BTDC; (b) 1600 r/min, 8 °CA BTDC

based on a detailed methane mechanism, an H_2/CO combustion model, and a NO_x formation mechanism. Sensitivity analysis and the PSO method were introduced to optimize the kinetic mechanism. The optimized COG-Mech consists of 33 species and 120 reactions, and can be divided into three parts: reduced methane, optimized H_2/CO, and reduced NO_x formation mechanisms.

Based on the models established with CHEMKIN code, the fundamental combustion characteristics simulated with kinetic mechanisms were investigated. The optimized COG-Mech was validated with experimental data from the literature, and compared with the most commonly used mechanism, GRI-Mech 3.0. The results from shock-tube experiments were used to validate the ignition delay times, and COG-Mech showed a significantly higher accuracy. The premixed flame data measured with different methods were used for the validation of laminar flame speeds, and both mechanisms showed good agreement with the experimental data, while some small differences existed.

Based on the engine test bench, the in-cylinder pressure and NO_x emission measured by combustion analyzer and FTIR spectrometer were used to validate the applicability of kinetic mechanism in engine simulations, and a 3D in-cylinder model coupled with COG-Mech was established with the open source software KIVA-CHEMKIN. The simulated in-cylinder pressure and NO_x emission showed good agreement with the experimental data.

References

Ahmed, S.S., Mauss, F., Moréac, G., *et al*., 2007. A comprehensive and compact n-heptane oxidation model derived using chemical lumping. *Physical Chemistry Chemical Physics*, **9**(9):1107-1126. http://dx.doi.org/10.1039/B614712G

Baulch, D.L., Cobos, C.J., Cox, R.A., *et al*., 1994. Evaluated kinetic data for combustion modeling. *Journal of Physical & Chemical Reference Data*, **23**(6):847-1033. http://dx.doi.org/10.1063/1.555953

Bhattacharjee, B., Schwer, D.A., Barton, P.I., *et al*., 2003. Optimally-reduced kinetic models: reaction elimination in large-scale kinetic mechanisms. *Combustion & Flame*, **135**(3):191-208. http://dx.doi.org/10.1016/S0010-2180(03)00159-7

Bilger, R.W., Stårner, S.H., Kee, R.J., 1990. On reduced mechanisms for methane air combustion in nonpremixed flames. *Combustion & Flame*, **80**(2):135-149. http://dx.doi.org/10.1016/0010-2180(90)90122-8

Boni, A.A., Penner, R.C., 1977. Sensitivity analysis of a mechanism for methane oxidation kinetics. *Combustion Science & Technology*, **15**(3-4):99-106. http://dx.doi.org/10.1080/00102207708946775

Bougrine, S., Richard, S., Nicolle, A., *et al*., 2011. Numerical study of laminar flame properties of diluted methane-hydrogen-air flames at high pressure and temperature using detailed chemistry. *International Journal of Hydrogen Energy*, **36**(18):12035-12047. http://dx.doi.org/10.1016/j.ijhydene.2011.06.053

Bowman, C.T., 1992. Control of combustion-generated nitrogen oxide emissions: technology driven by regulation. *Symposium (International) on Combustion*, **24**(1):859-878. http://dx.doi.org/10.1016/S0082-0784(06)80104-9

Davis, S.G., Law, C.K., 1998. Determination of and fuel structure effects on laminar flame speeds of C_1 to C_8 hydrocarbons. *Combustion Science & Technology*, **140**(1-6):427-449. http://dx.doi.org/10.1080/00102209808915781

Davis, S.G., Joshi, A.V., Wang, H., *et al*., 2005. An optimized kinetic model of H_2/CO combustion. *Proceedings of the Combustion Institute*, **30**(1):1283-1292. http://dx.doi.org/10.1016/j.proci.2004.08.252

Dong, C., Zhou, Q., Zhao, Q., 2009. Experimental study on the laminar flame speed of hydrogen/carbon monoxide/air mixtures. *Fuel*, **88**(10):1858-1863. http://dx.doi.org/10.1016/j.fuel.2009.04.024

Dong, C., Zhou, Q., Chen, X., *et al*., 2014. On the laminar flame speed of hydrogen, carbon monoxide, and natural gas mixtures with air: insights for a dual-fuel polygeneration system. *Energy Sources, Part A: Recovery, Utilization, and Environmental Effects*, **36**(4):393-401. http://dx.doi.org/10.1080/15567036.2010.538806

Dowdy, D.R., Smith, D.B., Taylor, S.C., 1991. The use of expanding spherical flames to determine burning velocities and stretch effects in hydrogen/air mixtures. *Symposium (International) on Combustion*, **23**(1):325-332. http://dx.doi.org/10.1016/S0082-0784(06)80275-4

Frassoldati, A., Faravelli, T., Ranzi, E., 2007. The ignition, combustion and flame structure of carbon monoxide/hydrogen mixtures. Note 1: detailed kinetic modeling of syngas combustion also in presence of nitrogen compounds. *International Journal of Hydrogen Energy*, **32**(15):3471-3485. http://dx.doi.org/10.1016/j.ijhydene.2007.01.011

Gaydon, A.G., Hurle, I.R., 1963. The Shock Tube in High-temperature Chemical Physics. Chapman & Hall, UK.

Gersen, S., Darmeveil, H., Levinsky, H., 2012. The effects of CO addition on the autoignition of H_2, CH_4 and CH_4/H_2 fuels at high pressure in an RCM. *Combustion & Flame*, **159**(12):3472-3475. http://dx.doi.org/10.1016/j.combustflame.2012.06.021

Golovitchev, V., 2002. The Mechanism of Iso-octane. Chalmers University of Technology. http://www.tfd.chalmers.se/~valeri/MECH/

Gu, X.J., Haq, M.Z., Lawes, M., *et al*., 2000. Laminar burning velocity and Markstein lengths of methane–air mixtures. *Combustion & Flame*, **121**(1-2):41-58.

http://dx.doi.org/10.1016/S0010-2180(99)00142-X

Halter, F., Chauveau, C., Djebaili-Chaumeix, N., *et al*., 2005. Characterization of the effects of pressure and hydrogen concentration on laminar burning velocities of methane–hydrogen–air mixtures. *Proceedings of the Combustion Institute*, **30**(1):201-208. http://dx.doi.org/10.1016/j.proci.2004.08.195

He, F., Li, Y.M., Wu, H.B., *et al*., 2013. A performance study of coke oven gas vehicle. *Advanced Materials Research*, **724-725**:1201-1205. http://dx.doi.org/10.4028/www.scientific.net/AMR.724-725.1201

Huang, J., Hill, P.G., Bushe, W.K., 2004. Shock-tube study of methane ignition under engine-relevant conditions: experiments and modeling. *Combustion & Flame*, **136**(1-2):25-42. http://dx.doi.org/10.1016/j.combustflame.2003.09.002

Huang, Z., Zhang, Y., Zeng, K., *et al*., 2006. Measurements of laminar burning velocities for natural gas–hydrogen–air mixtures. *Combustion & Flame*, **146**(1-2):302-311. http://dx.doi.org/10.1016/j.combustflame.2006.03.003

Hughes, K.J., Turányi, T., Clague, A.R., *et al*., 2001. Development and testing of a comprehensive chemical mechanism for the oxidation of methane. *International Journal of Chemical Kinetics*, **33**(9):513-538. http://dx.doi.org/10.1002/kin.1048

Jazbec, M., Fletcher, D.F., Haynes, B.S., 2000. Simulation of the ignition of lean methane mixtures using CFD modelling and a reduced chemistry mechanism. *Applied Mathematical Modelling*, **24**(8-9):689-696. http://dx.doi.org/10.1016/S0307-904X(00)00012-3

Kalitan, D.M., Mertens, J.D., Crofton, M.W., *et al*., 2007. Ignition and oxidation of lean CO/H_2 fuel blends in air. *Journal of Propulsion & Power*, **23**(6):1291-1301. http://dx.doi.org/10.2514/1.28123

Kee, R.J., Grcar, J.F., Smooke, M.D., 1985. PREMIX: a Fortran Program for Modeling Steady Laminar One-dimensional Premixed Flames. Technical Report No. SAND85-8249. Sandia National Laboratories, Livermore, USA.

Kee, R.J., Rupley, F.M., Meeks, E., *et al*., 1996. CHEMKIN-III: a FORTRAN Chemical Kinetics Package for the Analysis of Gas-phase Chemical and Plasma Kinetics. Technical Report No. SAND96-8216. Sandia National Laboratories, Livermore, USA. http://dx.doi.org/10.2172/481621

Kennedy, J., Eberhart, R., 1995. Particle swarm optimization. Proceedings of IEEE International Conference on Neural Networks. http://dx.doi.org/10.1109/icnn.1995.488968

Konnov, A.A., 2000. Detailed Reaction Mechanism for Small Hydrocarbons Combustion. Release 0.5. http://homepages.vub.ac.be/akonnov

Krejci, M.C., Mathieu, O., Vissotski, A.J., *et al*., 2013. Laminar flame speed and ignition delay time data for the kinetic modeling of hydrogen and syngas fuel blends. *Journal of Engineering for Gas Turbines & Power*, **135**(2):021503. http://dx.doi.org/10.1115/1.4007737

Kuo, K.K., 1986. Principles of Combustion. John Wiley & Sons, New York, USA.

Kwon, O.C., Faeth, G.M., 2001. Flame/stretch interactions of premixed hydrogen-fueled flames: measurements and predictions. *Combustion and Flame*, **124**(4):590-610. http://dx.doi.org/10.1016/S0010-2180(00)00229-7

Li, J., Zhao, Z., Kazakov, A., *et al*., 2007. A comprehensive kinetic mechanism for CO, CH_2O, and CH_3OH combustion. *International Journal of Chemical Kinetics*, **39**(3):109-136. http://dx.doi.org/10.1002/kin.20218

Li, S.C., Williams, F.A., 2002. Reaction mechanisms for methane ignition. *Journal of Engineering for Gas Turbines & Power*, **124**(3):471-480. http://dx.doi.org/10.1115/1.1377871

Liu, X., Liu, J.F., Zhao, W.B., *et al*., 2007. The particle swarm optimization algorithm restraining local optimum. *Journal of Daqing Petroleum Institute*, **31**(6):101-104 (in Chinese). http://dx.doi.org/10.3969/j.issn.2095-4107.2007.06.029

Lu, T., Law, C.K., 2006. Linear time reduction of large kinetic mechanisms with directed relation graph: n-heptane and iso-octane. *Combustion & Flame*, **144**(1-2):24-36. http://dx.doi.org/10.1016/j.combustflame.2005.02.015

Metghalchi, M.A.K.J., Keck, J.C., 1980. Laminar burning velocity of propane-air mixtures at high temperature and pressure. *Combustion & Flame*, **38**:143-154. http://dx.doi.org/10.1016/0010-2180(80)90046-2

Michael, J.V., Su, M.C., Sutherland, J.W., *et al*., 2002. Rate constants for $H+O_2+M\rightarrow HO_2+M$ in seven bath gases. *The Journal of Physical Chemistry A*, **106**(21):5297-5313. http://dx.doi.org/10.1021/jp020229w

Mittal, G., Sung, C.J., Yetter, R.A., 2006. Autoignition of H_2/CO at elevated pressures in a rapid compression machine. *International Journal of Chemical Kinetics*, **38**(8):516-529. http://dx.doi.org/10.1002/kin.20180

Montgomery, C.J., Swensen, D.A., Harding, T.V., *et al*., 2002. A computational problem solving environment for creating and testing reduced chemical kinetic mechanisms. *Advances in Engineering Software*, **33**(2):59-70. http://dx.doi.org/10.1016/S0965-9978(01)00054-0

Mueller, M.A., Yetter, R.A., Dryer, F.L., 1999. Flow reactor studies and kinetic modeling of the $H_2/O_2/NO_x$, and $CO/H_2O/O_2/NO_x$ reactions. *International Journal of Chemical Kinetics*, **31**(10):705-724. http://dx.doi.org/10.1002/(SICI)1097-4601(1999)31:10<705::AID-JCK4>3.3.CO;2-R

Olm, C., Zsély, I.G., Varga, T., *et al*., 2015. Comparison of the performance of several recent syngas combustion mechanisms. *Combustion & Flame*, **162**(5):1793-1812. http://dx.doi.org/10.1016/j.combustflame.2014.12.001

Petersen, E.L., Davidson, D.F., Hanson, R.K., 1999. Kinetics modeling of shock-induced ignition in low-dilution CH_4/O_2 mixtures at high pressures and intermediate temperatures. *Combustion & Flame*, **117**(1-2):272-290. http://dx.doi.org/10.1016/S0010-2180(98)00111-4

Petersen, E.L., Kalitan, D.M., Barrett, A.B., *et al*., 2007. New

syngas/air ignition data at lower temperature and elevated pressure and comparison to current kinetics models. *Combustion & Flame*, **149**(1-2):244-247. http://dx.doi.org/10.1016/j.combustflame.2006.12.007

Qin, W.J., Xie, M.Z., Jia, M., *et al*., 2014. Large eddy simulation and proper orthogonal decomposition analysis of turbulent flows in a direct injection spark ignition engine: cyclic variation and effect of valve lift. *Science China Technological Sciences*, **57**(3):489-504. http://dx.doi.org/10.1007/s11431-014-5472-x

Ra, Y., Reitz, R.D., 2008. A reduced chemical kinetic model for IC engine combustion simulations with primary reference fuels. *Combustion & Flame*, **155**(4):713-738. http://dx.doi.org/10.1016/j.combustflame.2008.05.002

Rabitz, H., Kramer, M., Dacol, D., 1983. Sensitivity analysis in chemical kinetics. *Annual Review of Physical Chemistry*, **34**:419-461. http://dx.doi.org/10.1146/annurev.pc.34.100183.002223

Ruscic, B., Feller, D., Dixon, D.A., *et al*., 2001. Evidence for a lower enthalpy of formation of hydroxyl radical and a lower gas-phase bond dissociation energy of water. *ChemInform*, **32**(15):1-4. http://dx.doi.org/10.1002/chin.200115014

Saxena, P., Williams, F.A., 2006. Testing a small detailed chemical-kinetic mechanism for the combustion of hydrogen and carbon monoxide. *Combustion & Flame*, **145**(1-2):316-323. http://dx.doi.org/10.1016/j.combustflame.2005.10.004

Scholte, T.G., Vaags, P.B., 1959. Burning velocities of mixtures of hydrogen, carbon monoxide and methane with air. *Combustion & Flame*, **3**:511-524. http://dx.doi.org/10.1016/0010-2180(59)90057-4

Sher, E., Refael, S., 1988. A simplified reaction scheme for the combustion of hydrogen enriched methane/air flame. *Combustion Science & Technology*, **59**(4-6):371-389. http://dx.doi.org/10.1080/00102208808947106

Shioji, M., Eguchi, S., Kitazaki, M., *et al*., 2004. Knock characteristics and performance in an SI engine with hydrogen and natural-gas blended fuels. SAE Technical Paper 2004-01-1929. http://dx.doi.org/10.4271/2004-01-1929

Smith, G.P., Golden, D.M., Frenklach, M., *et al*., 1999. GRI-Mech 3.0. University of California, Berkeley, USA. http://combustion.berkeley.edu/gri-mech/version30/text30.html

Smooke, M.D., 1991. Reduced Kinetic Mechanisms and Asymptotic Approximations for Methane-Air Flames: a Topical Volume. Springer Berlin Heidelberg. http://dx.doi.org/10.1007/BFb0035362

Sun, H., Yang, S.I., Jomaas, G., *et al*., 2007. High-pressure laminar flame speeds and kinetic modeling of carbon monoxide/hydrogen combustion. *Proceedings of the Combustion Institute*, **31**(1):439-446. http://dx.doi.org/10.1016/j.proci.2006.07.193

Tan, Z., Reitz, R.D., 2006. An ignition and combustion model based on the level-set method for spark ignition engine multidimensional modeling. *Combustion & Flame*, **145**(1-2):1-15. http://dx.doi.org/10.1016/j.combustflame.2005.12.007

Turányi, T., Nagy, T., Zsély, I.G., *et al*., 2012. Determination of rate parameters based on both direct and indirect measurements. *International Journal of Chemical Kinetics*, **44**(5):284-302. http://dx.doi.org/10.1002/kin.20717

Turns, S.R., 1996. An Introduction to Combustion: Concepts and Applications. McGraw-Hill, USA. http://dx.doi.org/10.1036/007235044X

Varga, L., Szabó, B., Zsély, I.G., *et al*., 2011. Numerical investigation of the uncertainty of Arrhenius parameters. *Journal of Mathematical Chemistry*, **49**(8):1798-1809. http://dx.doi.org/10.1007/s10910-011-9859-7

Wang, H., Frenklach, M., 1991. Detailed reduction of reaction mechanisms for flame modeling. *Combustion & Flame*, **87**(3-4):365-370. http://dx.doi.org/10.1016/0010-2180(91)90120-Z

Warnatz, J., 2000. Hydrocarbon oxidation high-temperature chemistry. *Pure & Applied Chemistry*, **72**(11):2101-2110. http://dx.doi.org/10.1351/pac200072112101

中文概要

题　目： 清洁车用代用燃料焦炉气化学反应机理的简化与优化

目　的： 化学反应机理在内燃机计算流体动力学（CFD）仿真中起关键作用。基于敏感性分析与粒子群寻优算法，本文旨在提出适用于内燃机 CFD 仿真的焦炉气化学反应机理，为焦炉气在内燃机上的应用研究提供条件。

创新点： 1. 结合敏感性分析与离子群寻优算法，对化学反应机理参数进行了优化；2. 建立了焦炉气化学反应机理，可准确仿真滞燃期、层流火焰速度、缸内压力变化和 NO_x 生成。

方　法： 1. 根据简单碳氢燃料机理结构，搭建焦炉气化学反应机理（图 1）；2. 通过敏感性分析，获得在燃烧中起关键作用的化学反应（图 2 和 3）；3. 通过粒子群寻优算法，对上述关键化学反应的动力学参数进行优化（图 4 和 5）；4. 通过数值仿真，验证机理的准确性（图 6~13、16 和 17）。

结　论： 1. 根据敏感性定义，搭建的敏感性分析模型可准确地识别在燃烧过程中起关键作用的化学反应；2. 基于粒子群寻优算法搭建的优化模型可对化学反应的动力学参数进行合理优化；3. 优化后得到的焦炉气化学反应机理可准确预测滞燃期与层流火焰速度以及模拟内燃机缸内压力变化与 NO_x 生成。

关键词： 焦炉气；化学反应机理；敏感性分析；粒子群寻优；内燃机；计算流体力学仿真

Appendix A: Extended reactions and reaction rate coefficients

Reactions considered	A	b	E
$CH_3+OH=CH_2O+H_2$	8.00×10^{12}	0.0	0.0
$CH_3+O_2=CH_3O_2$	2.13×10^{58}	−15.0	17018.0
$C_2H_5O=CH_2O+CH_3$	1.00×10^{15}	0.0	21606.0
$CH_3O+HO_2=CH_2O+H_2O_2$	1.20×10^{13}	0.0	0.0
$CH_3O+CH_3=CH_2O+CH_4$	2.41×10^{13}	0.0	0.0
$CH_3O_2H=CH_3O+OH$	6.46×10^{14}	0.0	42996.0
$CH_3O_2+CH_3=CH_3O+CH_3O$	3.00×10^{13}	0.0	−1200.0
$CH_3O_2+H_2O_2=CH_3O_2H+HO_2$	2.40×10^{12}	0.0	9942.0
$CH_3O_2+CH_2O=CH_3O_2H+HCO$	2.00×10^{12}	0.0	11663.0
$CH_3O_2+CH_4=CH_3O_2H+CH_3$	1.80×10^{11}	0.0	18475.0
$C_2H_5+O_2=C_2H_5O_2$	1.00×10^{12}	0.0	0.0
$C_2H_5O_2+CH_2O=C_2H_5O_2H+HCO$	2.00×10^{12}	0.0	11663.0
$C_2H_5O_2H=C_2H_5O+OH$	1.00×10^{16}	0.0	42977.0
$CH_3O_2+HO_2=CH_3O_2H+O_2$	4.60×10^{10}	0.0	2600.0
$CH_3O_2+CH_3O_2=O_2+2CH_3O$	3.70×10^{11}	0.0	2200.0

A: pre-exponential factor (kg/(m·s)); b: temperature factor; E: activation energy (J/mol)

Appendix B: Reduced COG mechanism

	Reactions considered	A	b	E
1	$H+O_2=O+OH$	2.64×10^{16}	−0.7	17041.0
2	$O+H_2=H+OH$	4.59×10^{4}	2.7	6260.0
3	$OH+H_2=H+H_2O$	1.73×10^{8}	1.5	3430.0
4	$OH+OH=O+H_2O$	3.97×10^{4}	2.4	−2110.0
5	$H+H+M=H_2+M$	1.78×10^{18}	−1.0	0.0
6	$H+H+H_2=H_2+H_2$	9.00×10^{16}	−0.6	0.0
7	$H+H+H_2O=H_2+H_2O$	5.62×10^{19}	−1.2	0.0
8	$H+H+CO_2=H_2+CO_2$	5.50×10^{20}	−2.0	0.0
9	$H+OH+M=H_2O+M$	4.40×10^{22}	−2.0	0.0
10	$O+H+M=OH+M$	9.43×10^{18}	−1.0	0.0
11	$O+O+M=O_2+M$	1.20×10^{17}	−1.0	0.0
12	$H+O_2(+M)=HO_2(+M)$	5.12×10^{12}	0.4	0.0
13	$H_2+O_2=HO_2+H$	5.92×10^{5}	2.4	53502.0
14	$OH+OH(+M)=H_2O_2(+M)$	1.11×10^{14}	−0.4	0.0
15	$HO_2+H=O+H_2O$	3.97×10^{12}	0.0	671.0
16	$HO_2+H=OH+OH$	7.48×10^{13}	0.0	295.0
17	$HO_2+O=OH+O_2$	4.00×10^{13}	0.0	0.0
18	$HO_2+OH=O_2+H_2O$ DUP (duplicate)	2.38×10^{13}	0.0	−500.0
19	$HO_2+OH=O_2+H_2O$ DUP	1.00×10^{16}	0.0	17330.0
20	$HO_2+HO_2=O_2+H_2O_2$ DUP	1.30×10^{11}	0.0	−1630.0
21	$HO_2+HO_2=O_2+H_2O_2$ DUP	3.66×10^{14}	0.0	12000.0
22	$H_2O_2+H=HO_2+H_2$	6.05×10^{6}	2.0	5200.0
23	$H_2O_2+H=OH+H_2O$	2.41×10^{13}	0.0	3970.0
24	$H_2O_2+O=OH+HO_2$	9.63×10^{6}	2.0	3970.0
25	$H_2O_2+OH=HO_2+H_2O$ DUP	2.00×10^{12}	0.0	427.0

26	$H_2O_2+OH=HO_2+H_2O$ DUP	2.67×10^{41}	−7.0	37600.0
27	$CO+O(+M)=CO_2(+M)$	1.36×10^{10}	0.0	2384.0
28	$CO+OH=CO_2+H$ DUP	8.00×10^{11}	0.1	7352.0
29	$CO+OH=CO_2+H$ DUP	8.78×10^{10}	0.0	−16.0
30	$CO+O_2=CO_2+O$	1.12×10^{12}	0.0	47700.0
31	$CO+HO_2=CO_2+OH$	3.01×10^{13}	0.0	23000.0
32	$HCO+H=CO+H_2$	1.20×10^{14}	0.0	0.0
33	$HCO+O=CO+OH$	3.00×10^{13}	0.0	0.0
34	$HCO+O=CO_2+H$	3.00×10^{13}	0.0	0.0
35	$HCO+OH=CO+H_2O$	3.02×10^{13}	0.0	0.0
36	$HCO+M=CO+H+M$	1.87×10^{17}	−1.0	17000.0
37	$HCO+H_2O=CO+H+H_2O$	2.24×10^{18}	−1.0	17000.0
38	$HCO+O_2=CO+HO_2$	1.20×10^{10}	0.8	−727.0
39	$O+CH_2=H+HCO$	8.00×10^{13}	0.0	0.0
40	$O+CH_3=H+CH_2O$	8.43×10^{13}	0.0	0.0
41	$O+CH_4=OH+CH_3$	1.02×10^{9}	1.5	8600.0
42	$O+CH_2O=OH+HCO$	3.90×10^{13}	0.0	3540.0
43	$O+C_2H_2=CO+CH_2$	1.02×10^{7}	2.0	1900.0
44	$O+C_2H_4=CH_3+HCO$	1.92×10^{7}	1.8	220.0
45	$O+C_2H_5=CH_3+CH_2O$	1.32×10^{14}	0.0	0.0
46	$O+C_2H_6=OH+C_2H_5$	8.98×10^{7}	1.9	5690.0
47	$O_2+CH_2O=HO_2+HCO$	1.00×10^{14}	0.0	40000.0
48	$H+CH_2(+M)=CH_3(+M)$	2.50×10^{16}	−0.8	0.0
49	$H+CH_3(+M)=CH_4(+M)$	1.27×10^{16}	−0.6	383.0
50	$H+CH_4=CH_3+H_2$	6.60×10^{8}	1.6	10840.0
51	$H+HCO(+M)=CH_2O(+M)$	1.09×10^{12}	0.5	−260.0
52	$H+CH_2O(+M)=CH_3O(+M)$	5.40×10^{11}	0.5	2600.0
53	$H+CH_2O=HCO+H_2$	2.30×10^{10}	1.1	3275.0
54	$H+CH_3O=OH+CH_3$	3.20×10^{13}	0.0	0.0
55	$H+C_2H_2(+M)=C_2H_3(+M)$	5.60×10^{12}	0.0	2400.0
56	$H+C_2H_3(+M)=C_2H_4(+M)$	6.08×10^{12}	0.3	280.0
57	$H+C_2H_3=H_2+C_2H_2$	3.00×10^{13}	0.0	0.0
58	$H+C_2H_4(+M)=C_2H_5(+M)$	1.08×10^{12}	0.5	1820.0
59	$H+C_2H_4=C_2H_3+H_2$	1.32×10^{6}	2.5	12240.0
60	$H+C_2H_5(+M)=C_2H_6(+M)$	5.21×10^{17}	−1.0	1580.0
61	$H+C_2H_6=C_2H_5+H_2$	1.15×10^{8}	1.9	7530.0
62	$H_2+CO(+M)=CH_2O(+M)$	4.30×10^{7}	1.5	79600.0
63	$OH+CH_2=H+CH_2O$	2.00×10^{13}	0.0	0.0
64	$OH+CH_3=CH_2+H_2O$	5.60×10^{7}	1.6	5420.0
65	$OH+CH_4=CH_3+H_2O$	1.00×10^{8}	1.6	3120.0
66	$OH+CH_2O=HCO+H_2O$	3.43×10^{9}	1.2	−447.0
67	$OH+C_2H_2=CH_3+CO$	4.83×10^{-4}	4.0	−2000.0
68	$OH+C_2H_3=H_2O+C_2H_2$	5.00×10^{12}	0.0	0.0
69	$OH+C_2H_4=C_2H_3+H_2O$	3.60×10^{6}	2.0	2500.0
70	$OH+C_2H_6=C_2H_5+H_2O$	3.54×10^{6}	2.1	870.0
71	$HO_2+CH_2=OH+CH_2O$	2.00×10^{13}	0.0	0.0
72	$HO_2+CH_3=O_2+CH_4$	1.00×10^{12}	0.0	0.0
73	$HO_2+CH_3=OH+CH_3O$	2.00×10^{13}	0.0	0.0
74	$HO_2+CH_2O=HCO+H_2O_2$	1.00×10^{12}	0.0	8000.0
75	$CH_2+O_2=OH+HCO$	1.32×10^{13}	0.0	1500.0
76	$CH_2+H_2=H+CH_3$	5.00×10^{5}	2.0	7230.0
77	$2CH_2=H_2+C_2H_2$	3.20×10^{13}	0.0	0.0
78	$CH_2+CH_3=H+C_2H_4$	4.00×10^{13}	0.0	0.0

79	$CH_2+CH_4=2CH_3$	2.46×10^{6}	2.0	8270.0
80	$CH_3+O_2=O+CH_3O$	2.68×10^{13}	0.0	28800.0
81	$CH_3+O_2=OH+CH_2O$	3.60×10^{10}	0.0	8940.0
82	$CH_3+H_2O_2=HO_2+CH_4$	2.45×10^{4}	2.5	5180.0
83	$2CH_3(+M)=C_2H_6(+M)$	2.12×10^{16}	−1.0	620.0
84	$2CH_3=H+C_2H_5$	4.99×10^{12}	0.1	10600.0
85	$CH_3+HCO=CH_4+CO$	2.65×10^{13}	0.0	0.0
86	$CH_3+CH_2O=HCO+CH_4$	3.32×10^{3}	2.8	5860.0
87	$CH_3+C_2H_4=C_2H_3+CH_4$	2.27×10^{5}	2.0	9200.0
88	$CH_3+C_2H_6=C_2H_5+CH_4$	6.14×10^{6}	1.7	10450.0
89	$CH_3O+O_2=HO_2+CH_2O$	4.28×10^{-13}	7.6	−3530.0
90	$C_2H_3+O_2=HCO+CH_2O$	3.98×10^{12}	0.0	−240.0
91	$C_2H_4(+M)=H_2+C_2H_2(+M)$	8.00×10^{12}	0.4	88770.0
92	$C_2H_5+O_2=HO_2+C_2H_4$	8.40×10^{11}	0.0	3875.0
93	$CH_3+OH=CH_2O+H_2$	8.00×10^{12}	0.0	0.0
94	$CH_3+O_2=CH_3O_2$	2.13×10^{58}	−15.0	17018.0
95	$C_2H_5O=CH_2O+CH_3$	1.00×10^{15}	0.0	21606.0
96	$CH_3O+HO_2=CH_2O+H_2O_2$	1.20×10^{13}	0.0	0.0
97	$CH_3O+CH_3=CH_2O+CH_4$	2.41×10^{13}	0.0	0.0
98	$CH_3O_2H=CH_3O+OH$	6.46×10^{14}	0.0	42996.0
99	$CH_3O_2+CH_3=CH_3O+CH_3O$	3.00×10^{13}	0.0	−1200.0
100	$CH_3O_2+H_2O_2=CH_3O_2H+HO_2$	2.40×10^{12}	0.0	9942.0
101	$CH_3O_2+CH_2O=CH_3O_2H+HCO$	2.00×10^{12}	0.0	11663.0
102	$CH_3O_2+CH_4=CH_3O_2H+CH_3$	1.80×10^{11}	0.0	18475.0
103	$C_2H_5+O_2=C_2H_5O_2$	1.00×10^{12}	0.0	0.0
104	$C_2H_5O_2+CH_2O=C_2H_5O_2H+HCO$	2.00×10^{12}	0.0	11663.0
105	$C_2H_5O_2H=C_2H_5O+OH$	1.00×10^{16}	0.0	42977.0
106	$CH_3O_2+HO_2=CH_3O_2H+O_2$	4.60×10^{10}	0.0	2600.0
107	$CH_3O_2+CH_3O_2=O_2+2CH_3O$	3.70×10^{11}	0.0	2200.0
108	$N+NO=N_2+O$	3.50×10^{13}	0.0	330.0
109	$N+O_2=NO+O$	2.65×10^{12}	0.0	6400.0
110	$N+OH=NO+H$	7.33×10^{13}	0.0	1120.0
111	$N+CO_2=NO+CO$	1.90×10^{11}	0.0	3400.0
112	$N_2O+O=N_2+O_2$	1.40×10^{12}	0.0	10810.0
113	$N_2O+O=NO+NO$	2.90×10^{13}	0.0	23150.0
114	$N_2O+H=N_2+OH$	4.40×10^{14}	0.0	18880.0
115	$N_2O+OH=N_2+HO_2$	2.00×10^{12}	0.0	21060.0
116	$N_2O+M=N_2+O+M$	1.30×10^{11}	0.0	59620.0
117	$NO+HO_2=NO_2+OH$	2.11×10^{12}	0.0	−480.0
118	$NO_2+O=NO+O_2$	3.90×10^{12}	0.0	−240.0
119	$NO_2+H=NO+OH$	1.32×10^{14}	0.0	360.0
120	$NO+O+M=NO_2+M$	1.06×10^{20}	−1.4	0.0

Appendix C: Revised reaction parameters

Reactions considered		*A*	*b*	*E*
3	$OH+H_2=H+H_2O$	1.00×10^{8}	1.5	3430.0
22	$H_2O_2+H=HO_2+H_2$	7.50×10^{13}	2.0	37500.0
29	$CO+OH=CO_2+H$	4.00×10^{10}	0.0	−16.0
31	$CO+HO_2=CO_2+OH$	7.53×10^{12}	0.0	23000.0
82	$CH_3+H_2O_2=HO_2+CH_4$	1.15×10^{4}	2.5	5180.0
83	$2CH_3(+M)=C_2H_6(+M)$	7.00×10^{15}	−1.0	620.0